Single-particle fluctuations and directional correlations in driven hard-sphere glasses

Mandal, S.; Chikkadi, V.; Nienhuis, B.; Raabe, R.; Schall, P.; Varnik, F.

DOI
10.1103/PhysRevE.88.022129

Publication date
2013

Document Version
Final published version

Published in
Physical Review E

Single-particle fluctuations and directional correlations in driven hard-sphere glasses

Suvendu Mandal,[1] Vijaykumar Chikkadi,[2] Bernard Nienhuis,[2] Dierk Raabe,[1] Peter Schall,[2] and Fathollah Varnik[1,3,*]

[1]*Max-Planck Institut für Eisenforschung, Max-Planck Strasse 1, 40237 Düsseldorf, Germany*

[2]*Institute of Physics, University of Amsterdam, Science Park 904, 1098 XH Amsterdam, The Netherlands*

[3]*Interdisciplinary Centre for Advanced Materials Simulation (ICAMS), Ruhr-Universität Bochum, Stiepeler Strasse 129, 44801 Bochum, Germany*

(Received 13 May 2013; published 19 August 2013)

Via event-driven molecular dynamics simulations and experiments, we study the packing-fraction and shear-rate dependence of single-particle fluctuations and dynamic correlations in hard-sphere glasses under shear. At packing fractions above the glass transition, correlations increase as shear rate decreases: the exponential tail in the distribution of single-particle jumps broadens and dynamic four-point correlations increase. Interestingly, however, upon decreasing the packing fraction, a broadening of the exponential tail is also observed, while dynamic heterogeneity is shown to decrease. An explanation for this behavior is proposed in terms of a competition between shear and thermal fluctuations. Building upon our previous studies [Chikkadi *et al.*, Europhys. Lett. **100**, 56001 (2012)], we further address the issue of anisotropy of the dynamic correlations.

DOI: 10.1103/PhysRevE.88.022129 PACS number(s): 61.43.Fs, 62.20.F−, 82.70.Dd, 83.80.Hj

I. INTRODUCTION

The relation between the dynamics of structural rearrangement and response in driven amorphous materials has been a subject of growing interest in the past decade [1–6]. A central issue in this context is the growth of spatial correlations upon approaching the glass transition (see, e.g., [7–12] and references therein). In quiescent glasses, it is well established that upon approaching the glass transition, dynamic correlations grow; this is manifested in an increase of the dynamic susceptibility [13] as well as strongly non-Gaussian displacement distributions. However, extensive simulations and experiments showed that along with the sudden increase of the macroscopic viscosity and relaxation time, the dynamic correlation length remains relatively small, limited to a few particle diameters [8,10–12]. The situation changes when the glass is driven by applied shear that forces structural rearrangements [14]; such external driving can lead to avalanchelike plastic response [4,5]. It is then interesting to elucidate how the dynamics crosses over from the thermal regime of supercooled liquids to the athermal limit of strongly driven glasses. Besides the magnitude of correlations, an important issue concerns their direction dependence: because shear introduces obvious directionality, this should reflect itself in the microscopic fluctuations or their correlations, setting them apart from thermally induced correlations. Indeed, our recent simulations and experiments revealed a transition from isotropic to anisotropic correlations with increasing importance of shear [15]; this observation is in qualitative agreement with the anisotropic correlations observed in the athermal limit of two-dimensional Lennard-Jones glasses [16] and at finite temperatures [17]. These anisotropic correlations might play a central role in the shear-banding transition of glasses as suggested in [14].

Hard-sphere systems have been widely used as model systems to elucidate the dynamics of glasses because of their conceptual simplicity. These systems have been particularly valuable to obtain experimental insight into the microscopic dynamics. While the small molecular length scales make the direct observation of microscopic fluctuations in molecular glasses a difficult task, the situation is more favorable in the case of colloidal particles with diameters of the order of 1 μm thanks to the development of modern confocal microscopy techniques [18,19]. This technique has been fine tuned in recent years to allow simultaneous tracking of the trajectories of a large number of particles (up to $N = 10^6$). We have recently combined this promising experimental tool with computer simulations to study the emergence of anisotropy of correlations in hard-sphere colloidal glasses [15]. A systematic investigation of the effect of shear versus packing fraction (the fraction of the system volume occupied by particles) on the microscopic fluctuations and their correlations, however, remained elusive; this would provide deeper insight into the nature of the dynamic arrest of glasses and the response to applied shear.

In this paper, we build upon our earlier studies and investigate the shear-rate and packing-fraction dependence of dynamic fluctuations and correlations in hard-sphere glasses. We present event-driven molecular dynamics simulations and experimental observations of particle dynamics in sheared supercooled liquids and glasses at shear rates from the thermal to the shear-dominated regime.

We find that upon decreasing the shear rate, the exponential tail of the single-particle displacement distributions broadens, and we show that this broadening is linked to the increase of dynamic heterogeneity [20,21] as proposed in [22]. In contrast to this, upon increasing the packing fraction at constant shear rate, dynamic correlations grow but the exponential tail of the displacement distributions becomes narrower. We interpret this in terms of a competition between shear-induced and inherent thermally induced dynamics. Finally, we address the question of the direction dependence of spatial correlations. We find a consistent direction dependence in both simulations and experiments: isotropic correlations in the thermal regime go over into anisotropic correlations when shear dominates the relaxation. Besides this agreement, however, the decay

*fathollah.varnik@rub.de

of correlations has a different functional form. While an exponential decay perfectly describes our simulation data, a power-law behavior is found in the experiments. This longer-range power-law decay is in qualitative agreement with the much larger correlation volume measured in the experiments. A possible reason for this discrepancy can be hydrodynamic interactions, which are present in the experiments, but not accounted for in the simulations.

The paper is organized as follows: In Sec. II, we provide details of the simulations and the experimental system. We then present simulation results on the structure and single-particle displacements in Sec. III A, investigate the relation between single-particle displacements and dynamic correlations in Sec. III B, and elucidate the functional form of the correlations in Sec. III C. Section IV is devoted to the experimental results. We investigate the structure and single-particle displacements in Sec. IV A and the dynamic correlations in Sec. IV B, and elucidate the functional form in Sec. IV C. Final discussions and conclusions are then presented in Sec. V.

II. SIMULATION MODEL AND EXPERIMENTAL SYSTEM

Our simulation model is a polydisperse (11%) hard-sphere system of mass $m = 1$ and average diameter $\sigma = 0.8$. We perform event-driven molecular dynamics (MD) simulations using DynamO [23], and we do not observe any crystallization. Lengths are measured in units of the average particle diameter σ. We use Lees-Edwards boundary conditions to have a time-dependent shear strain $\gamma = t\dot{\gamma}$, where $\dot{\gamma}$ varies from 4×10^{-5} to 10^{-2}. With periodic boundary conditions on the coordinates x_i, y_i, and z_i in an $L \times L \times L$ system, the position of particle i in a box with strain γ is defined as $r_i = (x_i + \gamma z_i, y_i, z_i)$. The packing fraction is tuned from below to above the glass transition point, which, for the present polydisperse system, is located at a packing fraction of $\phi_g \approx 58.5\%$ [24]. The quiescent properties of this system have been studied extensively in [25]. The temperature is fixed at $T = 1$ via velocity rescaling. We present all the measurements after 100% shearing to ensure that the system has reached the steady state.

For the experimental measurements, we use a hard-sphere suspension consisting of sterically stabilized polymethylmethacrylate particles suspended in a mixture of cycloheptyl bromide and cis-decalin that matches both the density and refractive index of the particles. The particles have a diameter of $\sigma = 1.3\ \mu$m, with a polydispersity of 7%. The particle volume fraction is fixed at $\phi \sim 0.6$. We apply shear with constant shear rates in the range of 1.5×10^{-5} to 2.2×10^{-4} s^{-1}, corresponding to Péclet numbers $\dot{\gamma}\tau$ between 0.3 and 2.2, respectively. Here, the structural relaxation time $\tau = 2 \times 10^4$ s was determined from the mean-square displacement of the particles. More experimental details can be found in [14].

III. SIMULATION RESULTS

A. Structure versus single-particle dynamics

We first elucidate the glass structure and single-particle displacements in the simulations. From linear response theory it is well known that in a system under shear the pair distribution function cannot be fully isotropic, since it would then correspond to zero stress. Some, even though slight, amount of anisotropy is thus always present in the structure of a sheared system. In order to highlight this property, we determine via both computer simulations and experiments the pair distribution function $g(r,\theta)$ along different spatial directions. Given that a particle is at the origin of the coordinate system, $g(r,\theta)$ is the probability density for finding another particle a distance r apart from the origin along the direction θ with respect to the flow (in the shear plane). Similarly to previous experiments on colloidal suspensions [26] and computer simulations on a Lennard-Jones glass [3], we observe in Fig. 1(a) an enhanced peak along the compression axis ($\theta = 135^\circ$) and a weaker one along the extension axis ($\theta = 45^\circ$). Furthermore, not quite unexpectedly, the peak position along the compression (extension) axis is shifted to slightly smaller (larger) distances. Interestingly, no detectable difference could be found for $g(r)$ along the x, y, and z directions.

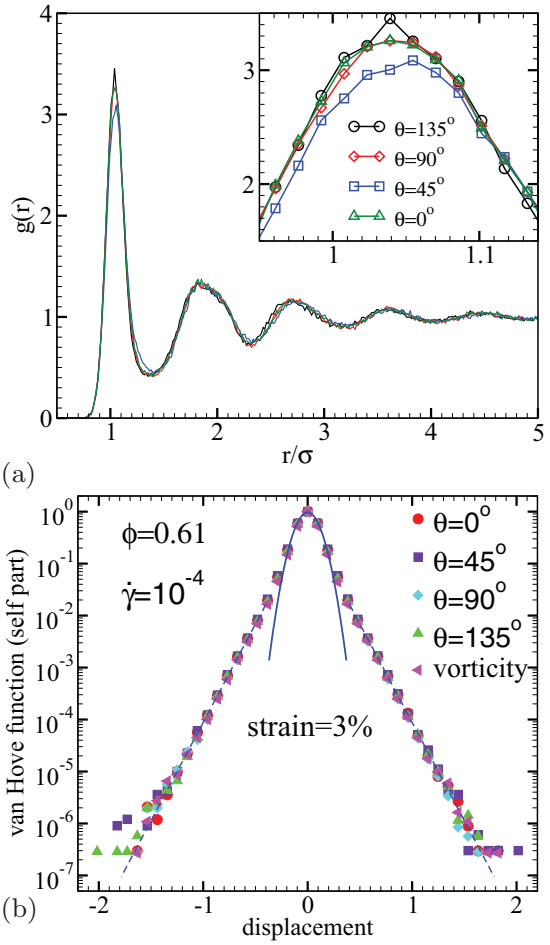

FIG. 1. (Color online) (a) The pair distribution function along various directions. Interestingly, the difference between the principal coordinate directions ($\theta = 0^\circ$ and $\theta = 90^\circ$) is hardly detectable. Albeit small, the anisotropy is, however, well resolved when comparing the extension and compression directions ($\theta = 45^\circ$ and $\theta = 135^\circ$) in the shear plane (spanned by the flow and shear gradient directions). (b) Distribution function of single-particle displacements $G_s(\Delta x, \Delta t)$, determined along different directions as indicated. Obviously, no signature of anisotropy is visible in this quantity. Solid lines are exponential fits. The dashed line is a quasi-Gaussian fit.

Since the local packing structure of an amorphous system strongly influences its dynamic behavior [27], it is interesting to check whether this anisotropy has an effect on the distribution of single-particle displacements. In this context, it must be mentioned that, in the presence of flow, the displacement of a particle consists of an affine part, which reflects the deterministic motion with the macroscopic velocity field, and a nonaffine part, which constitutes the random part of the dynamics. Of course, when investigating the single-particle distribution, it is the nonaffine part of particle displacements which is used.

In order to obtain nonaffine displacements, we proceed as follows [28]. For each particle, we follow nearest neighbors in time and determine the best affine tensor $\boldsymbol{\epsilon}$ that transforms the nearest-neighbor vectors $\mathbf{d}_i = \mathbf{r}_i - \mathbf{r}_0$ over the time interval δt. This is done by minimizing $D^2 = (1/n)\sum_{i=1}^{n}[\mathbf{d}_i(t+\delta t) - (\mathbf{I}+\boldsymbol{\epsilon})\cdot\mathbf{d}_i(t)]^2$, where $\mathbf{I}$ is the identity matrix. D^2 reflects the mean-square deviation from a local affine deformation, and is an excellent measure of local plasticity [29]. The nonaffine displacements of the particles are determined both (i) via subtraction of the local flow,

$$d\boldsymbol{r}^{\mathrm{na}} = \mathbf{r}(t+\delta t) - \mathbf{r}(t) - \int_0^t dt'\mathbf{u}(t',\mathbf{r}(t')), \qquad (1)$$

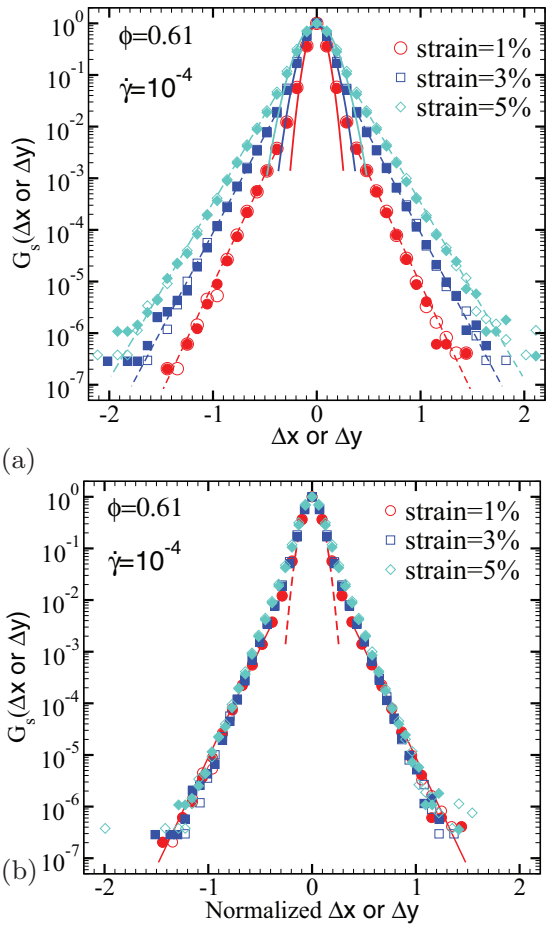

FIG. 2. (Color online) (a) The self part of the van Hove function along the flow and vorticity directions (x and y) for different strain intervals. (b) Same as in (a) but now normalized by the width of the distribution function.

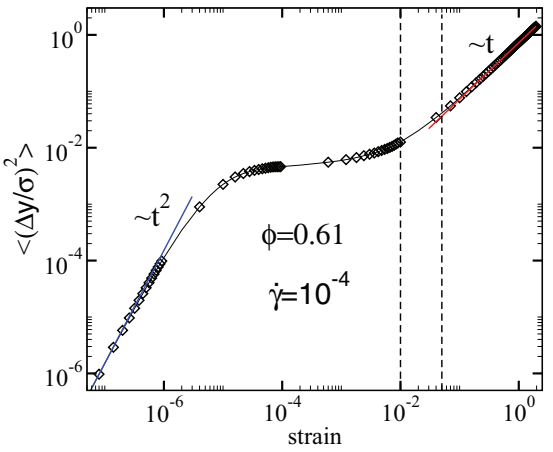

FIG. 3. (Color online) Mean-squared displacements at a packing fraction of $\phi = 0.61$ and a shear rate of $\dot{\gamma} = 10^{-4}$. The vertical dashed lines mark the range of strains used in Fig. 2.

where $\mathbf{u}(t,\mathbf{r}(t))$ is a coarse-grained displacement field [28], and (ii) as $d\boldsymbol{r}^{\mathrm{na}} = \mathbf{r}(t+\delta t) - \mathbf{r}(t) - \boldsymbol{\epsilon}\cdot\mathbf{r}(t)$. It is assumed in (ii) that the coordinate center is at rest. We have verified that these two definitions give identical results as long as the shear is homogeneous across the channel [30]. In the general case of heterogeneous shear, however, the first definition is used.

Applying the above procedure, we have determined the distribution of nonaffine displacements, also called the self part of the van Hove function $G_s(\Delta x,\Delta t)$, along various spatial directions. As seen from Fig. 1(b), in contrast to the pair distribution, the single-particle displacements seem to be quite insensitive to shear-induced anisotropy, in agreement with previous reports [31]. In marked contrast to this observation, as will be shown below, the situation is quite different for the spatial correlations of the displacements.

When computing the displacement distributions, a question arises regarding a possible dependence of the results on the selected time or strain interval. Here we show that there is a range of strain intervals where the shape of $G_s(\Delta x,\Delta t)$ is essentially unchanged (Fig. 2). As a survey of the mean-square displacement (MSD) (see Fig. 3) clearly shows, the selected strain interval corresponds to the time domain where particles start to leave the cage but still are partially trapped (departure from the plateau in the MSD). We expect significant changes in $G_s(\Delta x,\Delta t)$ for both shorter and longer strain intervals. For shorter times, particles move essentially unperturbed along straight lines (ballistic motion) and since the velocity distribution is a Maxwellian, the distribution of the displacements $\Delta\mathbf{r} = \mathbf{v}\Delta t$ is also a Maxwellian (Gaussian). In the limit of long times, on the other hand, particles leave the cage and their motion becomes uncorrelated to that of their neighbors so that again a Gaussian distribution is established [22].

B. Single-particle displacements and dynamic heterogeneity

We are now in the position to study the effect of shear rate and packing fraction on the displacement distribution. The effect of shear rate is demonstrated in Fig. 4(a). We observe a Gaussian central part and a perfect exponential decay at large displacements; this exponential tail broadens

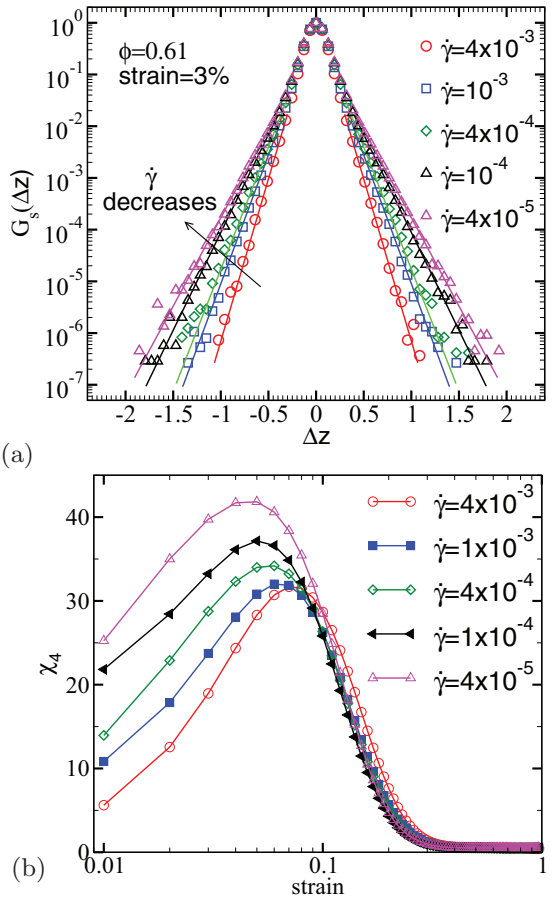

FIG. 4. (Color online) Effect of shear rate on (a) $G_s(\Delta z)$ and (b) χ_4. The exponential tail becomes broader as $\dot{\gamma}$ decreases. This is accompanied by a corresponding increase of the maximum value of the dynamic susceptibility, a measure of dynamic heterogeneity in the system.

with decreasing shear rate. Broad non-Gaussian tails in the self part of the van Hove function have also been observed in [22]. The exponential form of the tail and its universal character have been recently addressed in [22] where a simple model based on the idea of dynamic heterogeneity has been proposed, which could reproduce this important feature with only a few fit parameters. The central idea behind the approach proposed in [22] is that the particles in the system can be divided into slow and fast groups. While the former perform essentially vibrational motion in the cage formed by their neighbors, the more mobile particles make comparably large jumps (of the order of the cage size). Despite the fact that the distributions of single-particle displacements in both cases are Gaussian (with different underlying length and time scales), an exponential tail with logarithmic corrections can be deduced for the $G_s(\Delta x, \Delta t)$ of the entire system [22].

This motivates us to seek an interpretation of our observations in terms of dynamic heterogeneity. The observed broadening would imply that dynamic heterogeneity becomes enhanced at lower $\dot{\gamma}$. A way to test this idea is to compute the so-called correlation volume for dynamic correlations. There are a number of ways of determining the correlation volume. Two well-known possibilities are the overlap function [12] and the peak value of the four-point susceptibility of density fluctuations, χ_4 [21]. Here, we choose the second option and determine $\chi_4 = N[\langle f_q^2(t)\rangle - \langle f_q(t)\rangle^2]$. In this expression, N is the particle number and $f_q(t) = N^{-1}\sum_{i=1}^{N} \exp\{i\mathbf{q}\cdot[\mathbf{r}_i(t) - \mathbf{r}_i(0)]\}$ is the incoherent scattering function at wave vector $\mathbf{q}$. Results on χ_4 are plotted in Fig. 4(b). In agreement with the above-described picture, the maximum value of χ_4 increases with decreasing shear rate. This observation is also in line with early studies of Yamamoto and Onuki who showed evidence for the growing length of dynamic correlations upon decreasing shear rate in a binary mixture of soft-core particles [32].

The effect of packing fraction is addressed in Fig. 5. We show G_s and χ_4 for a range of packing fractions at a fixed shear rate of $\dot{\gamma} = 10^{-4}$. Again, a Gaussian central part and a perfect exponential decay at large displacements are found in all the cases shown. Note that, upon decreasing the packing fraction, one expects a *decrease* of correlations but an increase of particle mobility. We thus expect that the probability for a jump of a given length will increase upon decreasing ϕ, while the maximum of χ_4 will decrease. This expectation is confirmed by the data shown in Fig. 5.

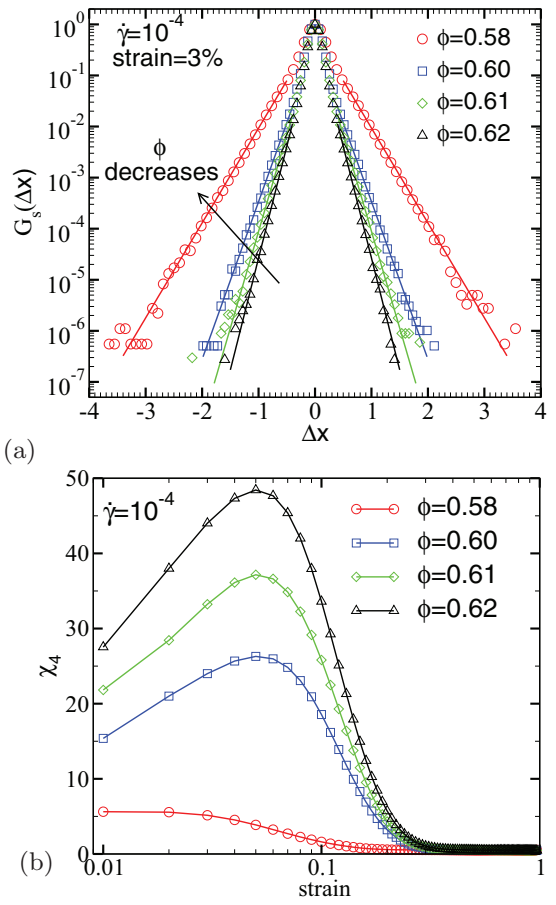

FIG. 5. (Color online) Effect of packing fraction on (a) $G_s(\Delta x)$ and (b) χ_4. The exponential tail in $G_s(\Delta x, \Delta t)$ becomes broader as ϕ increases. This is accompanied by a growth of the maximum value of χ_4.

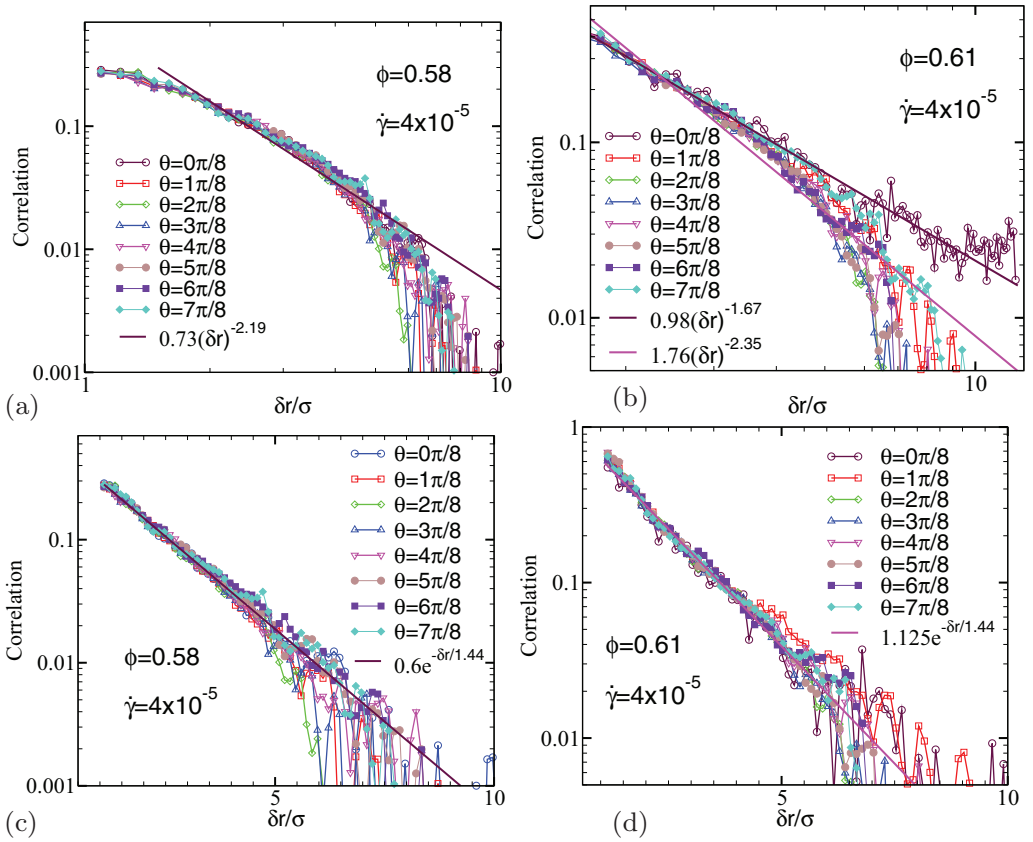

FIG. 6. (Color online) Correlation of plastic activity in the shear (x,z) plane along different spatial directions with respect to the flow. In order to better highlight the functional dependence, the same data are presented both in a log-log scale (a) and (b) and in a log-linear plot (c) and (d). In (d), the angle-dependent long-time limit of $C_{D^2}(\Delta\mathbf{r})$ is subtracted from the data.

C. Spatial correlations of displacements

In this section, we focus on the direction dependence of dynamic correlations. To do so, we use the scalar quantity D^2 introduced above, which is actually a byproduct of the calculation of nonaffine displacements. In order to study spatial correlation between nonaffine displacements, we define the function [14]

$$C_{D^2}(\Delta\mathbf{r}) = \frac{\langle D^2(\mathbf{r}+\Delta\mathbf{r})D^2(\mathbf{r})\rangle - \langle D^2(\mathbf{r})\rangle^2}{\langle D^2(\mathbf{r})^2\rangle - \langle D^2(\mathbf{r})\rangle^2}. \qquad (2)$$

The function $C_{D^2}(\Delta\mathbf{r})$ provides a measure of correlations between nonaffine displacements at two points in space separated by a vector $\Delta\mathbf{r} = (\delta x, \delta y, \delta z)$. Here, we determine the directional dependence of this correlation function by projecting the distance vector $\Delta\mathbf{r}$ along different directions with respect to the flow. To avoid unnecessary fluctuations, we average the correlation over the angular width $\pi/60$. It is also worth mentioning that, as shown above in the case of $G_s(\Delta x, \Delta t)$, we have explicitly checked that the correlation function C_{D^2} is insensitive to the specific value of the strain $\delta\gamma$, as long as it is in the intermediate regime (data not shown).

Results on C_{D^2} are depicted in Fig. 6 for two characteristic packing fractions of $\phi = 0.58$ (supercooled state) and $\phi = 0.61$ (glass) for a shear rate of $\dot{\gamma} = 4 \times 10^{-5}$. As seen from this plot, the correlation of plastic activity is fully isotropic in the supercooled state, while marked anisotropy is visible in the glassy phase ($\phi = 61$). This is an important observation since it tells us that, even in the steady state where a colloidal glass is considered to be completely shear melted, it is possible to distinguish a glass from a supercooled liquid by purely dynamical measurements, i.e., without referring to any static property of the system.

In order to highlight the functional form of $C_{D^2}(\Delta\mathbf{r})$, we have illustrated the above data both in log-linear and in log-log scale. As visible from panels (a) and (b), strong deviations from the power law are observed both in the supercooled state and in the glass. This is in line with our previous report at a slightly higher shear rate [15]. Interestingly, plotting the same data in the log-linear scale reveals perfect exponential decay both in the supercooled state [Fig. 6(c)] and in the glassy phase [Fig. 6(d)]. We are not aware of any theoretical explanation for this exponential decay, and will show below that this in fact contrasts with the experimental observations. A possible interpretation of the different behavior of correlations in simulations and experiments is also given below.

IV. EXPERIMENTAL RESULTS

A. Structure versus single-particle displacements

We complement our simulations with experimental measurements of particle displacements in colloidal glasses. We first elucidate changes in the glass structure under shear by showing experimentally measured pair distribution functions

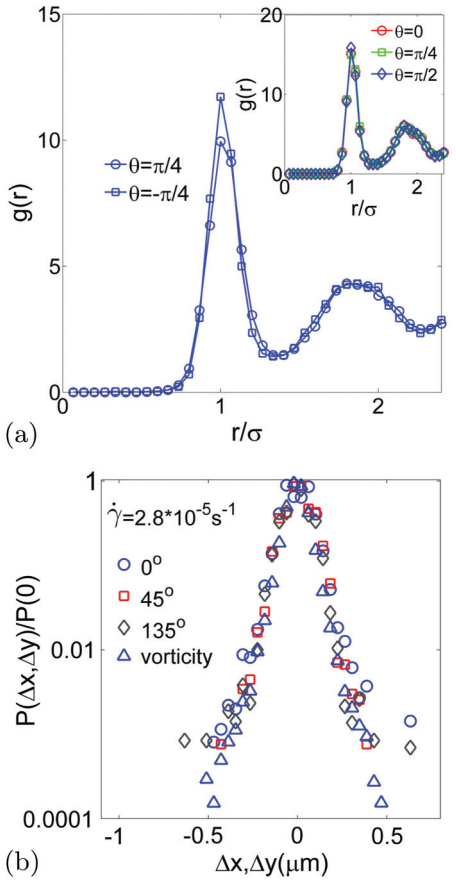

FIG. 7. (Color online) Experimental pair distribution function (a) and particle displacements (b) at a shear rate of $\dot{\gamma}\tau = 2.2$. The main panel in (a) shows the pair distribution function along the extension $(-\pi/4)$ and compression $(\pi/4)$ directions in the shear plane. A clear difference is observed. The inset shows the pair distribution function in the flow-vorticity plane. No significant difference between the directions is observed. (b) Particle displacements in the shear plane along the indicated directions with respect to the flow axis, as well as along the vorticity direction. Good overlap is observed.

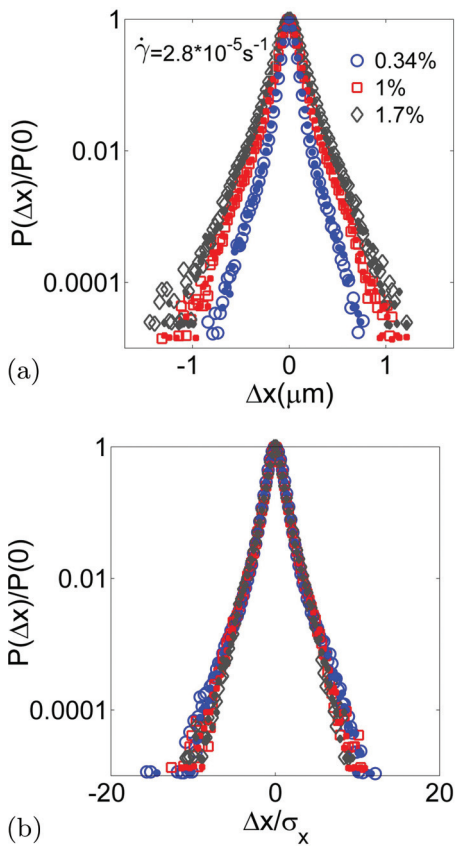

FIG. 8. (Color online) Experimentally measured particle displacements for increasing strain intervals. (a) Probability of particle displacements along the flow (open symbols) and vorticity (closed symbols) directions. (b) Same as in (a), but now normalized by the width of the distribution. The robust shape of the distribution function indicates robust behavior of the glass in the investigated time domain.

in Fig. 7(a). As in the simulations, in Fig. 7(a), main panel, we observe an enhanced peak along the compression direction, and a weaker one along the dilation direction, demonstrating a small distortion of the structure in the shear plane. On the other hand, no significant difference is observed in the flow-vorticity plane, as shown in the inset, again in agreement with the simulations. Note that because of the lower resolution of the confocal microscope in the vertical (flow gradient) direction, the absolute peak values in the main panel and inset are different. This is also the reason why we cannot directly compare directions with different inclinations to the vertical (flow gradient) direction. Nevertheless, comparison of directions with the same inclination to the vertical axis such as those shown in Fig. 7(a) is meaningful, and indeed shows a small structural distortion similar to the simulations.

Despite the small anisotropy of the structure, the displacements of the particles are surprisingly isotropic, again in agreement with the simulations. To show this, we determine the nonaffine displacements by subtracting contributions from the mean flow according to Eq. (1). We show the nonaffine displacements resolved along various directions with respect to the flow direction in Fig. 7(b). The data show that the distributions overlap, indicating that the single-particle displacements are isotropic. This is further confirmed when we investigate displacements for different strain intervals; the corresponding distributions of displacements, resolved along the flow and vorticity directions, are indicated in Fig. 8. The data show that the two distributions overlap for all strain intervals, again indicating the isotropy of the single-particle displacements. In fact, as in the simulations, the displacement distributions remain robust for all investigated strain intervals as shown by the overlap of the rescaled curves in Fig. 8(b). The collapse of the data indicates that the strain intervals all probe a similar time domain, where the particles exhibit essentially similar diffusive characteristics. The mean-square displacement of the particles (data not shown) shows that this time domain corresponds to the onset of the diffusive regime, similarly to the regime addressed by the simulations, as shown in Fig. 3.

B. Single-particle displacements and dynamic heterogeneity

As in the simulations, we use the full time-dependent particle trajectories to determine the corresponding displacement distributions and their dynamic correlations. We plot the results for three different shear rates spanning Péclet

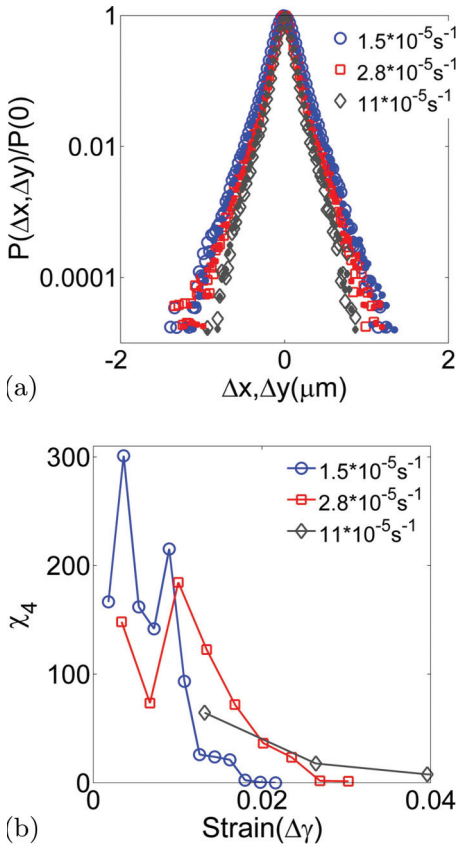

FIG. 9. (Color online) Experimentally measured displacement distribution (a) and dynamic susceptibility (b) plotted for increasing shear rate. The exponential tail in (a) becomes broader as $\dot{\gamma}$ decreases, as in the simulations. This is accompanied by an increase of the dynamic susceptibility as shown in (b).

numbers from 0.3 to 2.2 in Fig. 9. In agreement with the simulations, the displacement distributions show a broadening of the exponential tail with decreasing strain rate indicating increasing dynamic heterogeneity [Fig. 9(a)]. This increasing dynamic heterogeneity is confirmed by measurement of the dynamic susceptibility as shown in Fig. 9(b). At the smallest applied strain rate, the dynamic susceptibility rises to values larger than ∼300, indicating long-range correlated motion. Due to the limited acquisition speed of the three-dimensional imaging, however, small strain intervals are not accessible for the fastest strain rate and the maximum dynamic susceptibility lies outside the accessible window. While the results in Fig. 9 are in qualitative agreement with the simulations shown in Fig. 4, the absolute value of the dynamic susceptibility observed here is much larger than in the simulations. Obviously, this discrepancy cannot be explained by a packing-fraction effect as the overview over different packing fractions in Fig. 5(b) shows. A possible origin of this discrepancy is the hydrodynamic interaction between the particles which can have an influence on the collective dynamics at intermediate times, where the particles are rattling in the cage formed by their neighbors.

We are aware of the fact that the externally imposed shear rates studied in our experiments are far too low to give rise to macroscopically measurable lubrication forces so that the rheology of the system is largely independent of lubrication interactions. Regarding spatial correlations of particle displacements, however, the following argument may nevertheless be relevant. A colloidal particle of 1 μm diameter has a thermal velocity of the order of $v_{\text{thermal}} \sim \sqrt{k_B T/m_{\text{Colloid}}} \sim 10^{-3}$m/s. On the other hand, at high packing fractions considered in our studies, the surface-to-surface distance of two neighboring colloids is of the order of 10% of their diameter, i.e., $d_{12} \sim 10^{-7}$ m. A thermal motion of a colloidal particle with respect to its neighbor thus gives rise to a local shear rate of the order of $\dot{\gamma} \sim v_{\text{thermal}}/d_{12} \sim 10^4$/s, many orders of magnitude higher than the applied shear rate. The resulting hydrodynamic interactions can give rise to longer-range correlations. However, we shall emphasize that a colloidal particle has a quasideterministic motion only within a time interval comparable to the velocity autocorrelation time. Using standard relations, one finds $\tau_{\text{VACF}} \sim m/\zeta \sim \rho 4\pi R^3/3/(6\pi\eta R) = 2R^2/(9\nu)$ [where ζ is the friction coefficient, ρ is the density of the ambient fluid (solvent), η is the the solvent viscosity, R is the colloid's radius, and $\nu = \eta/\rho$ is the kinematic viscosity of the solvent]. Using typical values of $\nu = 10^{-6}$ m^2/s (water) and $R = 10^{-6}$ m, one obtains $\tau_{\text{VACF}} \approx 2 \times 10^{-7}$ s, corresponding to a distance of $\sim 2 \times 10^{-10}$ m. The question thus arises whether, within this deterministic part of the motion, the presence of the solvent gives rise to a correlation between the motion of two neighboring colloidal particles. Solvent-mediated momentum transfer across a channel of width L takes a time of the order of $\tau_{\text{momdiff}} \approx L^2/(8\nu)$ (see, e.g., [33]). We thus obtain $\tau_{\text{momdiff}}/\tau_{\text{VACF}} = (L/R)^2$. Using $L \approx 0.1R$, we see that the momentum transfer occurs sufficiently fast to give rise to a correlation between deterministic displacements of colloidal particles. It nevertheless remains to be clarified to what extent these correlations influence the type of correlations considered here, which relate displacements on significantly larger length scales.

Another point to be mentioned here is that the boundary conditions on the surface of a particle differ in simulations and experiments. While in experiments the stick boundary condition holds, perfect slip holds in simulations. As a result, tangential forces which may give rise to additional effects are absent in our simulations.

C. Spatial correlations

Finally, we elucidate the direction dependence of the dynamic correlations. We do so by determining the full three-dimensional correlation function from the measured particle trajectories, as was done previously in the simulations. Again, we use the nonaffine part of the displacements [Eq. (2)] to be unaffected by contributions from the mean flow. To smooth the experimental data, this time we choose angular bins of width $\pi/18$ around the specific directions. The resulting correlation functions are shown in Fig. 10. We distinguish two regimes: the thermal regime, where $\dot{\gamma}\tau < 1$ and particle motion is dominated by thermal fluctuations [Figs. 10(a) and 10(c)], and the regime $\dot{\gamma}\tau > 1$, where particle displacements are dominated by the applied shear [Figs. 10(b) and 10(d)]. The data reveal a characteristic change of the decay of correlations similar to that observed in the simulations: corre-

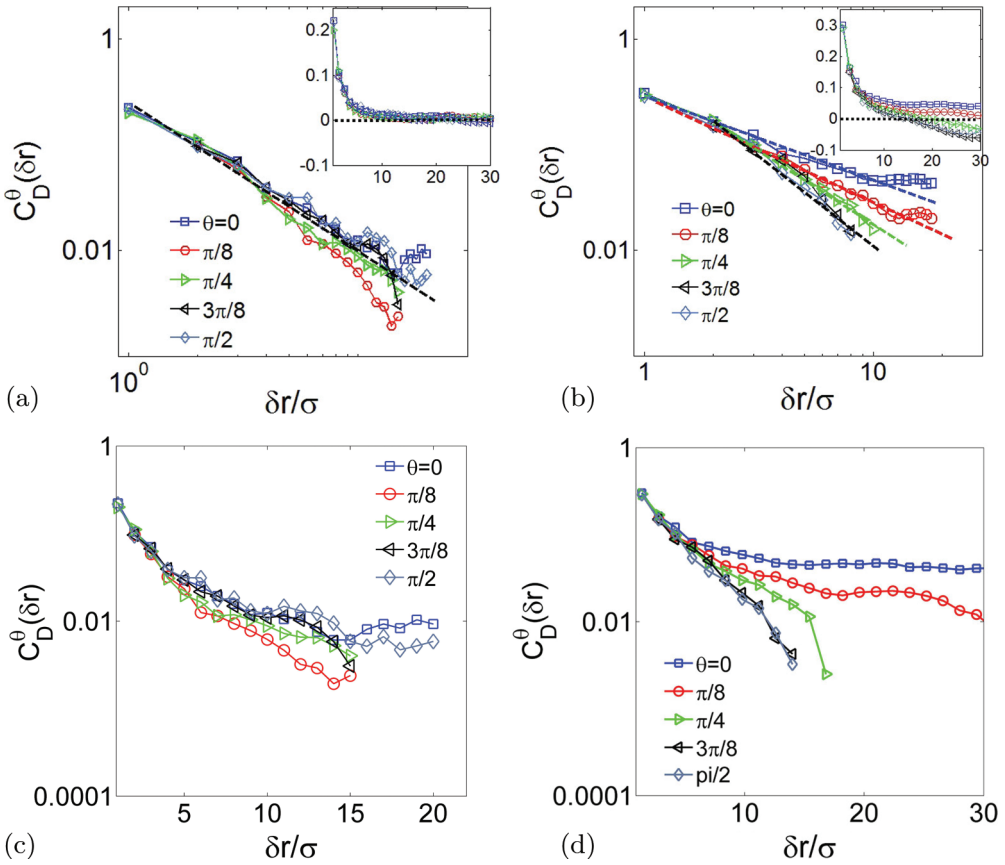

FIG. 10. (Color online) Experimental correlation functions of nonaffine displacements in the thermal ($\dot{\gamma}\tau = 0.3$) (a), (c) and shear-dominated ($\dot{\gamma}\tau = 2.2$) (b), (d) regimes, in double-logarithmic (upper row) and half-logarithmic (lower row) representations. The correlation functions are resolved along the indicated directions with respect to the flow direction in the shear plane.

lations exhibit isotropic decay in the thermal and anisotropic decay in the shear-dominated regime. In the latter case, the anisotropic decay is characterized by a slower decay in the flow and a faster decay in the flow-gradient direction. In contrast to the simulations, however, the functional forms of the decay appear different. The experimental data in Fig. 10 suggest a power-law decay of correlations, whereas the simulations indicate an exponential decay. This slower decay is in qualitative agreement with the larger values of χ_4 observed before: larger values of χ_4 indicate that dynamic correlations span more particles, and are therefore more extended in space, in agreement with the power-law decay observed in the experiments. As mentioned above, a possible reason for these longer-ranged spatial correlations may be solvent-mediated hydrodynamic interactions, which are present in experiments but not accounted for in our event-driven MD simulations.

V. CONCLUSION

Our simulations and experiments reveal interesting properties of displacement fluctuations in sheared glasses. While the glass structure and single-particle displacement fluctuations remain essentially isotropic, interesting features arise in the correlations of these displacements in terms of their anisotropy, volume-fraction, and strain-rate dependence. Our detailed analysis of simulation and experimental data shows that within the range of shear rates studied here, dynamic correlations grow with decreasing applied strain rate. This is mirrored in an increasing non-Gaussian behavior of the displacement distributions. Furthermore, correlations grow with increasing packing fraction. An interesting transition arises with respect to the symmetry of correlations: while correlations decay isotropically in the thermal regime, they become anisotropic when shear dominates the displacements. We find overall good qualitative agreement between the simulations and experiments; however, the range of dynamic correlations differs significantly as evidenced by a short-range exponential decay of correlations in the simulations, and a longer-range power-law-like decay in the experiments. A possible reason for this discrepancy is given in terms of local hydrodynamic interactions which are present in the colloidal system but fully absent in simulations. Further work is needed to investigate the origin of this discrepancy more closely. Since this interpretation is based on hydrodynamic effects arising from short-living cage-rattling motion of particles, temperature may also play a role since it directly influences this type of particle motion. Finally, we note that, within the intermediate time domain considered, our observations are robust. However, outside this time domain, in the ballistic regime of much smaller and the diffusive regime of much longer time scales, correlations should become short ranged again; this behavior should thus be similar to the behavior of dynamic correlations in quiescent glasses.

ACKNOWLEDGMENTS

S.M. is financially supported by the Max-Planck Society. P.S. acknowledges support by a VIDI Fellowship from the Netherlands Organization for Scientific Research (NWO). ICAMS acknowledges funding from its industrial sponsors, the state of North-Rhine Westphalia, and the European Commission in the framework of the European Regional Development Fund (ERDF).

[1] A. S. Argon, Acta Mater. **27**, 47 (1979).
[2] F. Varnik, L. Bocquet, J.-L. Barrat, and L. Berthier, Phys. Rev. Lett. **90**, 095702 (2003).
[3] K. Miyazaki, D. R. Reichman, and R. Yamamoto, Phys. Rev. E **70**, 011501 (2004).
[4] A. Lemaitre and C. Caroli, Phys. Rev. Lett. **103**, 065501 (2009).
[5] K. Martens, L. Bocquet, and J.-L. Barrat, Phys. Rev. Lett. **106**, 156001 (2011).
[6] S. Mandal, M. Gross, D. Raabe, and F. Varnik, Phys. Rev. Lett. **108**, 098301 (2012).
[7] C. Bennemann, C. Donati, J. Baschnagel, and S. C. Glotzer, Nature (London) **399**, 246 (1999).
[8] P. Scheidler, W. Kob, and K. Binder, Europhys. Lett. **59**, 701 (2002).
[9] J. Baschnagel and F. Varnik, J. Phys.: Condens. Matter **17**, R851 (2005).
[10] P. Ballesta, A. Duri, and L. Cipelletti, Nat. Phys. **4**, 550 (2008).
[11] F. Varnik and K. Binder, Int. J. Mater. Res. **100**, 1494 (2009).
[12] W. Kob, S. Roldan-Vargas, and L. Berthier, Nat. Phys. **8**, 164 (2012).
[13] L. Berthier, Physics **4**, 42 (2011).
[14] V. Chikkadi, G. Wegdam, D. Bonn, B. Nienhuis, and P. Schall, Phys. Rev. Lett. **107**, 198303 (2011).
[15] V. Chikkadi *et al.*, Europhys. Lett. **100**, 56001 (2012).
[16] C. E. Maloney and M. O. Robbins, Phys. Rev. Lett. **102**, 225502 (2009).
[17] A. Furukawa, K. Kim, S. Saito, and H. Tanaka, Phys. Rev. Lett. **102**, 016001 (2009).
[18] R. Besseling, E. R. Weeks, A. B. Schofield, and W. C. K. Poon, Phys. Rev. Lett. **99**, 028301 (2007).
[19] P. Schall, D. A. Weitz, and F. Spaepen, Science **318**, 1895 (2007).
[20] M. D. Ediger, Annu. Rev. Phys. Chem. **51**, 99 (2000).
[21] L. Berthier *et al.*, *Dynamical Heterogeneities in Glasses, Colloids, and Granular Media* (Oxford University Press, Oxford, 2011).
[22] P. Chaudhuri, L. Berthier, and W. Kob, Phys. Rev. Lett. **99**, 060604 (2007).
[23] M. Bannerman, R. Sargant, and L. Lue, J. Comput. Chem. **32**, 3329 (2011).
[24] P. N. Pussey *et al.*, Philos. Trans. R. Soc., A **367**, 4993 (2009).
[25] S. R. Williams, I. K. Snook, and W. van Megen, Phys. Rev. E **64**, 021506 (2001).
[26] X. Cheng, H. McCoy, J. N. Israelachvili, and I. Cohen, Science **333**, 1276 (2011).
[27] W. Götze, *Complex Dynamics of Glass-Forming Liquids-A Mode-Coupling Theory* (Oxford University, Oxford, 2009).
[28] C. Goldenberg, A. Tanguy, and J. L. Barrat, Europhys. Lett. **80**, 16003 (2007).
[29] M. L. Falk and J. S. Langer, Phys. Rev. E **57**, 7192 (1998).
[30] V. Chikkadi and P. Schall, Phys. Rev. E **85**, 031402 (2012).
[31] F. Varnik, in *Proceedings of the Fifth International Workshop on Complex Systems, Sendai, Japan, 2007*, edited by M. Tokuyama, I. Oppenheim, and H. Nishiyama, AIP Conf. Proc. No. 982 (American Institute of Physics, Melville, NY, 2007), p. 160.
[32] R. Yamamoto and A. Onuki, Phys. Rev. E **58**, 3515 (1998).
[33] F. Varnik, D. Dorner, and D. Raabe, J. Fluid Mech. **573**, 191 (2007).